Modeling Nanoparticle Generation in a Corona Charger

by

Wala Bkari

A thesis
presented to the University of Waterloo
in fulfillment of the
thesis requirement for the degree of
Master of Applied Science

in

Mechanical and Mechatronics Engineering

Waterloo, Ontario, Canada, 2018

AUTHOR'S DECLARATION

I hereby declare that I am the sole author of this thesis. This is a true copy of the thesis, including any required final revisions, as accepted by my examiners.

I understand that my thesis may be made electronically available to the public.

Abstract

The charging of airborne particles is an important process in both scientific studies and industrial applications. Recently, a new type of apparatus based on aerodynamic particle focusing and the corona charger technique was developed. These corona chargers produced an excellent agreement in particle sizing and charging for particles larger than 60 nm. Moreover, it was suggested that corona chargers could produce nanoparticles with sizes of less than 60 nm. As a result, a prototype was developed for the purpose of nanoparticle generation. The high voltage at the tip of the needle results in a non-uniform electric field between the two electrodes. In the corona charger that was developed by Saprykina [1], gold nanoparticles were generated. This study is focused on modeling the gold nanoparticles produced by the needle in the corona charger. The total amount of gold nanoparticles was calculated and compared with the experimental data. Results show that the mass of gold nanoparticles could be estimated when the spark happened at the needle in the corona charger. In addition, it was found that the mass depended on the polarity and the charging intensity.

Acknowledgments

First and, foremost, I must acknowledge the support and guidance of my supervisor, Dr. Zhongchao Tan. Without his dedicated efforts, this work would not have been finished. I must also recognize the continual efforts of my co-supervisor, Dr. Aiping Yu, Dr. Rahelah Givehchi, and Dr. Haiming Wang, and Maryam Razavi for their assistance.

I cannot express my gratitude and appreciation for the love and support from my parents Alwah Bakkari and Ali Bakari. Without their tireless efforts, I would never be where I am now. The same appreciation is extended to my dear sisters and brothers, especially Sara for her exceptional care. I must also acknowledge my friends, whether they are in Canada or Saudi Arabia, for their unwavering love and constant attention.

Last but not least, I would like to acknowledge the late Saudi King, King Abdel-Allah, may Allah have mercy on him, for offering me the enormous opportunity of a fully guaranteed scholarship, which has enabled me to undertake my graduate studies. Also, the continuous assistance from the Saudi Arabian Cultural Bureau in Canada is gratefully acknowledged, with special appreciation for Dr. Yousef Abu-Nada, for his supervision and help for all UW Saudi students, including myself.

Dedication

To my family.

Table of Contents

List of Figures

List of Tables

List of Symbols

Symbol	*Definition*
Au	Gold
ρ	density $\frac{kg}{m^3}$
μ	Dynamic gas viscosity $\frac{Kg}{m.s}$
M	Molar mass of the gas $\frac{kg}{mol}$
R	Universal gas constant $\frac{J}{K.mol}$
T	Temperature $°K$
StK	Stokes number is defining the size of the focused particles taken as 1
e	Elementary charge C
c	Constant determent by DMA
t	Time s
T_b	Boiling point
T_m	Melting point
T_s	Steady temperature 20 ℃
k	Thermal conductivity $(\frac{jols}{sec} * \frac{1}{cm*C})$
s	Specific heat $(\frac{jouls}{gram*C})$
L	Latent heat $\frac{J}{g}$
b	Constant depends on the losses of energy
g	Constant depends on the radiation of energy

H_v	Enthalpy of evaporation g/J
H_m	Enthalpy of melting g/J
C_{pl}	The energy needed to heat the liquid to boiling point $(J/gram * (°K))$
C_{ps}	Average heat capacitance for solid $(J/gram * (°K))$
Vf	Gas velocity m/s
Q	Volume flow rate 1.4 lpm m^3/s
I	Ion Current A

Chapter 1. Introduction

1.1 Background

Environmental risk assessment is one of the most significant research interests due to its profound effect on human beings. Increasing air pollution has also caused concern over the potential negative impact on human health and the environment. It is notable that tremendous air emissions surround our civilization and result in global warming and numerous health problems for humans. Air pollution occurs when unwanted material exists in the surrounding air, which could be inhaled, primarily resulting in lung diseases. Nanotechnology has been developing rapidly, and is likely to play a key role in the discovery and improvement of technologies that would help reduce air emissions. Therefore, we can observe nanotechnology becoming more involved in several fields such as medicine, science, and electronics.

Additionally, air pollution consists of airborne particles with a diverse composition including nitrates, sulfates, elemental and organic carbon, polycyclic aromatic hydrocarbons, biological compounds, and metals. Particulate matter commonly refers to the particles that can be suspended in the atmosphere, which are particles with a diameter of $10\ \mu m$ or less, along with the other fine particles with diameters of $2.5\ \mu m$ or less. Moreover, ultrafine particles may be formed in nanotechnology applications. Various technologies have been developed for the measurement of particle size distribution; generally, optical measuring methods work for aerosol particles larger than $100\ nm$, and smaller ones are detected by an electrical method. Nano aerosols comprise over 95% of particulate matter when the particles' number concentration is considered [2]. This fact emphasizes the importance of measuring

nanoparticles' number concentration rather than their mass concentration. Nanoparticles have a large surface area to volume ratio, which leads to a higher surface reactivity and other unique properties [3]. Surface area is a widely accepted property in studies of the toxicity of nanoparticles [4]. The numerical simulation of the motion of particles within corresponding force fields is a handy tool, which drastically reduces the cost, time, and effort needed for the design process. An overview of nanoparticle generating methods such as atomization, spray, flame, and evaporation condensation - one of the conventional technologies that combines high efficiency, easy access and low cost - are presented. Ideally, a generator is expected to produce a constant and reproducible output of stable aerosol particles with an adjustable size and concentration distribution. There are many nanoaerosol generators developed and commercially available based on different mechanisms. Depending on the mechanism used to generate ions, most unipolar chargers can be classified into corona, radioactive, and photoelectric. There are many factors involved in producing nanoparticles, including the high surface area to volume ratio that could provide a remarkable driving force for diffusion, especially at elevated temperatures. One of the methods is using a corona charger, which is used to generate and charge fine particles and to measure the ion current via an electrometer [5]. In addition, corona charge is applied to charge nanoparticles and filtering particles. Corona chargers are commercially available; however, the corona charger that was used in this paper was a homemade corona charger to experiment with aerosols.

1.2 Research Objectives

The main objectives of this thesis work were to gain a better understanding of the physics behind the nanoparticle generation in the corona charger and to obtain a better judgment of its maximum potential. A model was developed and compared with the experimental data for gold nanoparticle concentration in the [1] study.

1.3 Thesis Structure

The thesis is organized into four chapters. Chapter 1 is an introduction to the problem and objectives of the research. Chapter 2 contains a literature review of recent research conducted and an evaluation of this research. Chapter 3 provides a description of the corona charger, which was assembled by Saprykina [1], and theoretical analyses of the production of gold nanoparticles. Finally, Chapter 4 concludes the thesis and provides recommendations for future developments.

Chapter 2. Literature Review

2.1 Generating and Charging Aerosols

Aerosols are a collection of liquid or solid particles suspended in the air like smoke from power generation, primary particles from automobile exhaust, salt particles, and water droplets. The categorization of aerosols can be subdivided according to the physical form of the particles and their methods of generation. Furthermore, to study aerosols it is important to understand the behaviour of the particle motion, which is controlled by two forces: one is parallel to and the other is opposite of the particles [6].

Moreover, to generate aerosols there are many methods that depend on the purpose of the research. There is the powder form of generated aerosols, which could be broken down into smaller particles and released into the air. Aerosols are usually stable for at least a few seconds and, in some cases, may last a year or more. It is important to note that aerosols have many properties whether they originate from nature or from human creation.

Nanoparticles tend to agglomerate quickly when in contact with each other, whether in the starting powder or the generated aerosols. It is challenging to generate stable and reproducible aerosols composed of nanoparticle agglomerates ($< 100\ nm$) at concentrations and exposure times suitable for toxicological studies [7].The agglomeration of nanoparticles is a rapid process that is contingent on various factors, including concentration and primary particle size. As particle size decreases, the attractive force per unit mass becomes essential, which favours agglomeration. It is also challenging to produce agglomerates consisting of small particles.

Nanoaerosol generators have been developed and are commercially available based on different mechanisms. Several conditions affect the mechanisms of generating nanoparticles. The first is the surface condition, which means the roughness and porosity of the surface [8]. Second, the stress conditions, which means the load acting on the surface and its nature, that is, static or dynamic [8]. Thirdly, temperature dissipation; a temperature dissipation is very conclusive in ductile surfaces like metals. It is the dissipation or accumulation of the heat that results in the progressive adhesion of the wear particles that may or may not inhibit further wear [8]. Finally, contact condition is a reason that cannot be considered as entirely independent of other states, but it would be much simpler to find it separately while formulating the wear particle aerosol [9]. Another factor is the nature of the material properties like hardness, brittleness, and conductivity [9]. Particle charging can be organized by the charge of ions present, the charging mechanism, or the source of ions [8], as shown in Figure 1. The charge of ions present during charging can be unipolar or bipolar. There are some benefits of bipolar charging such as the possibility of establishing a charging equilibrium, the charge distribution is well defined, and the number of multiplied charged particles is limited. Nevertheless, the charging efficiency is limited, and this reduces the detection limit [10]. Additionally, unipolar charging will typically result in higher particle charging efficiencies because charged particles cannot recombine with particles of the opposite polarity [11].

Next, the ion source such as radioactivity depends on the $\beta \; and \; \alpha$ rays produced by different materials such as $Americium - 241 \; or \; Polonium - 210$ [8]. Particle charging is achieved by one of two mechanisms: field or diffusion. First, electric field charging cues field charging

[12]. Ions traveling along field lines collide with the particles and impart a charge to them. Eventually, enough ions are attached to the particle, preventing new ions from hitting them. In this state, the particle is said to be saturated. Small particles $< 1\ \mu m$ are not efficiently charged using this mechanism because they are not large enough to capture gas ions.

Diffusion charging is associated with the random motion of ions. It is related to the velocity of ions due to thermal kinetic energy. Their random movement causes collisions with particles and imparts a charge to them. This is the mechanism by which smaller particles $< 1\ \mu m$ are charged [8]. The corona source depends on the electric field from two electrodes. Another source is ultraviolet, which uses a $UV\ lamp$ to produce ions [1].

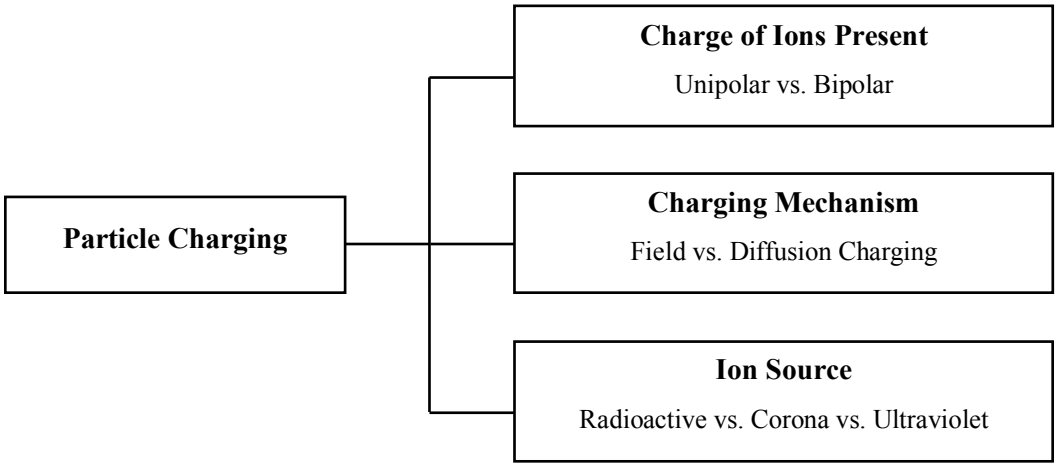

Figure 1: Classifications of Particle Charging [8]

2.2 Spark and Aerosols Generation

The spark discharge generator is a valid instrument used for generating aerosols. The pulse spark discharge method generates particles by evaporation and condensation of electrode material [13]. The spark generation is an electrical discharge between the two electrodes

possessing a low vapour pressure that leads to aerosol generation. In addition, there will be an inlet and outlet to pass the air flow to catch the generated and charged particles and to prevent the deposition of particles on the plate. The spark charger can use helium or argon atmosphere (inert atmosphere) to produce pure carbon or metallic aerosols [8]. The mean particle diameters of generated aerosols are differentiated between nanometers to micrometers.

Overall, the number size of generated nanoparticles is increased by raising the spark frequency, which means continually adding the voltage into the electrodes to produce multiple sparks. In some studies, the metallic electrode such as $Cu, Fe, or\ Zn$ was used to generate metallic aerosols and synthesize metallic particles [14]-[16]. The material of the electrode plays an important role in aerosol size due to their different energy losses. In addition, the distance also plays a role in the size distribution. Generated particles' purity is strongly related to the material of the electrodes. In the study by Tabrizi and colleagues [17], the erosion by micro spark discharge of metal particles was studied extensively by using a production rate via thermal conductivity, evaporation enthalpy and the boiling point of the materials shown in Table 1. It was thus possible to predict the mass amount of metal [17]. The mass increases with metals such as copper and nickel and decrease with stronger metals such as gold, tungsten, and iron [17]-[19]. Furthermore, the gases used in the chambers affect the mass amount [17]. Air flow and voltage frequency also have an impact on the total mass eroded [18].

Similar to the corona charger, spark generation is of special interest in producing monodisperse aerosols or particles of uniform size via electrical mobility analysis [17]. Spark charging is

mainly a process of gas phase generation, which is a common aspect of the corona charger. The corona charger is the more straightforward version of the spark generation system without considering any unique atmosphere [8]; However, the atmosphere and the purity of the materials are not found in the corona charger. The primary duty of the corona charger is to generate the ions to charge particles instead of creating nanoparticles.

Table 1: Different Metal Erosion at Spark Charger.

Metal	Amount	Distance between electrode	Scan Devises	References
Au, W, Ag	$W = 1 * 10^{-11} g$ $Ag = 2 * 10^{-11} g$ $Au = 2.3 * 10^{-11} g$	$.001(m)$	TEM	[17]
Au, W	Distribution size $Au = \ 20\ to\ 450$ $W = 14\ to\ 240$	$.015(m)$	AFM and SEM and EDX	[20]
Ag, Au, Ir	Transfer Coefficient $Au = .34 * 10^{-6} \frac{cm^3}{c}$ $Ag = .33 * 10^{-6} \frac{cm^3}{c}$ $Ir = .25 * 10^{-6} \frac{cm^3}{c}$	N/A	N/A	[18]
Platinum **Nickel** **Ir**	$platinum$ $= 3.3 * 10^{-9} gram$ $Nickel$ $= 6.6 * 10^{-9} gram$ Ir $= 11.8 * 10^{-9} gram$	$.002$ $-.003(m)$	N/A	[19]

2.2.1 Corona Charger

The corona charger is considered one of the most utilized techniques to produce high ion concentrations. Numerous designs of aerosol corona chargers have been reviewed and explained. These include both corona-wire and corona-needle chargers [21]. Likewise, some research was based on the polarity of the charge as a research focus. For example, one type of charger obtained unipolar ions through the separation of bipolar ions [22]. Moreover, several parameters should be considered when developing a corona charger. One of the parameters is particle dispersity such as polydispersity or monodispersity.

Another parameter is the material used to charge such as road test dust, sodium chloride ($NaCl$), metal, and filtered air. Furthermore, particle distribution, concentration, and flow rate are also parameters that could be extensively studied.

A variety of aerosol charging methods have been studied during the past three decades. The electrical properties of charged nanoparticles are fundamental in many aerosol studies and applications. Agglomerate particle synthesis [23], particle collection, and particle instrumentation are some examples of charged particle applications. These methods can be unipolar or bipolar. The most common conventional techniques to generate ions for unipolar diffusion charging in a gas are: corona discharge, photoemission from $UV - light$ radiation, and radiation from $X - ray$ sources. Numerous designs of unipolar aerosol corona chargers have been reviewed and explained including both corona-wire and corona-needle chargers [21]. Based on the unipolar source, unipolar particle chargers can be categorized into two types. Obtaining unipolar ions through the separation of bipolar ions is an undesirable method

because of the high cost and unsafe properties [22]. The charging efficiency of bipolar charging is low because of the recombination or neutralization of charged particles; on the other hand, unipolar charging has a higher ability because of the presence of ions of only one polarity [21]. Hewitt is one of the first developers of the corona-wire charger. A thin corona-wire charger was used to generate ions by corona discharge [24]. The results show that for the examined range of particles, $60\ to\ 700\ nm$, the particle loss is high for particles as small as $60\ nm$ [25]. In the corona wire, the losses of the nanoparticles are considered highly charged nanoparticles due to a high electric field. Some of this reduction can be achieved by introducing the surrounding sheath airflow at the boundary between the aerosol stream and the wall, which allows more space for the charged particles to flow through the charger without precipitating on the charger walls. However, the large sheath airflow results in dilution of the aerosols. Whitby developed a corona discharger that consists of a sharp needle electrode upstream of a sonic orifice [2]. A small orifice directs the unipolar ions out from the corona discharge. The particles were mixed with free ions in a chamber to be charged [2]. Hernandez and colleagues developed a unipolar charging of a nanometer-sized corona charger using a sharp point electrode to generate ions and applied the direct contact between electrodes [26]. The charging efficiency increased for larger particles and higher corona voltages up to a certain value [26]. Qi and colleagues used a DC corona charger and mixing type charger zone to obtain a higher extrinsic charging efficiency than other corona chargers [27]. The electrical mobility of negative ions is higher than that of positive ions, and it causes the lower extrinsic charging efficiency for negative ions. It has been shown that corona chargers generate unwanted

nanoparticles during operation that affect their applications [21], [25], [28], [29]. Medved investigated unipolar charging using ions generated by a platinum needle tip and forming an ion jet moving opposite to the particle jet as shown in Figure 2. There was particle generation of 0.3 particles per cubic centimeter for particles larger than 3 nm [30]. The unipolar charging was used in this experiment for removing the recombination effect of bipolar ions; however, passing filtered air through the corona charger causes the aerosols to be diluted [31], minimizing the number of the nanoparticle losses in the corona charger. It was found that both increasing the applied and electrical mobility of particles associated decreased particle diameter and the Reynolds number was affected by the losses of the nanoparticles. Intra and Tippayawong developed an ionizer that proved to be particularly useful as an aerosol charger for a positive and negative charge before the detector in an electrical aerosol detector [25]. A common mechanism for aerosol charging is diffusion charging. In this type of charging, particles are allowed to collide with ions and the charge carried by these ions is transferred to the particles. The process can be unipolar or bipolar, depending on the polarity of the ions colliding with the particles [11].

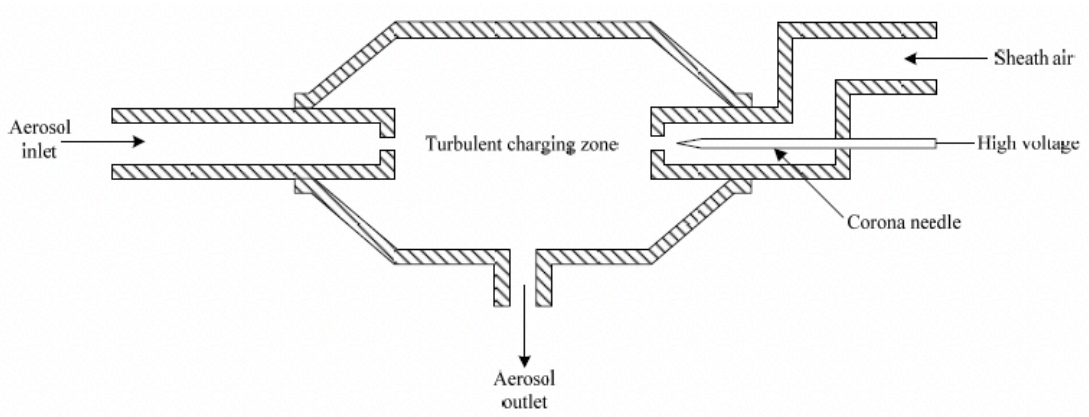

Figure 2: Schematic of Corona Charger Developed by [30].

In bipolar charging processes, the neutral particles are charged, while highly charged particles may be discharged by colliding with ions with different polarity [32]. This characteristic leads bipolar chargers to be used mainly for neutralizing highly charged particles. Furthermore, bipolar charging has very low efficiency for nanoparticles, which limits their application in charging nanometer-size particles [33]. For instance, the charging probability for $sub-20\ nm$ particles in bipolar charging is less than $0.01\ nm$ [34]-[36].

Comparing both charging methods, the unipolar method does not reach an equilibrium charge distribution and gives potentially higher efficiency. However, in bipolar diffusion charging, particles can grow by Brownian coagulation - an unwanted complication if the aerosol particle number concentration is above $10^7/cm^3$ [37]. A variety of unipolar chargers have been designed to achieve high charging efficiency [20], [33], [38], [39]. Bipolar diffusion charging has low efficiency due to the charge balance, which is 3.3% for positively charged $10\ nm$ particles and 5.7% for negatively charged particles. On the other hand, unipolar diffusion charging is characterized by the lack of balance, while bipolar diffusion charging, therefore,

potentially enables the attainment of a higher charging efficiency. As a result, some studies of unipolar charging have a higher particle efficiency than bipolar for nanoparticles less than $20\ nm$ in diameter [40]. However, unipolar charging has some weak points including the high possibility of losing particles during the charging process for all unipolar chargers. The particle loss in the charger is because the diffusion or electrostatic dispersion limits the application of particle charging [40].

A high-efficiency, high-throughput micro plasma-based aerosol charger for $sub-10-nm$ particles by minimizing the electrostatic loss of the charged particles was established. It was concluded that the electric flow rate does not have a notable impact on the charging efficiency [41].

2.2.2 The Evaporation-Condensation Method

The vapour-condensation method is a thermal process depending on heating and cooling materials such as metal and $NaCl$.

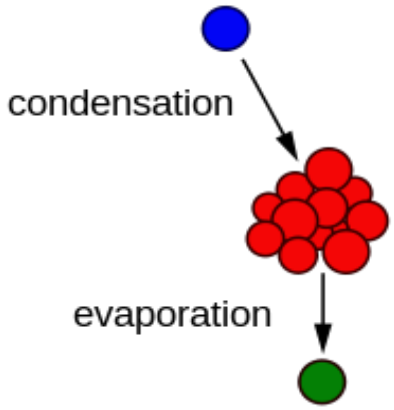

Figure 3: Evaporation and Condensation

The usual technique for the manufacturing of aerosols is evaporation of material in gas [6]. Nanoparticles are produced based on the principle of evaporation and condensation on nuclei and are characterized by generating solid nanoparticles such as $NaCl$, tungsten, gold, and silver [6]. This methodology is considered a highly recommended method because of the capability to control the nanoparticle shape and surface characteristics. The evaporation-condensation method has some disadvantages such as the need for high energy, large surfaces, and the long time needed to reach high temperatures; however, it has the most stable result for extended periods [22], and higher surface purity [17]. However, the primary drawback of this method is the furnace energy consumption and practical issues, like heating up and cooling down times [42]. Evaporation and condensation technology could affect the structure of the atoms in the material, affecting the physical properties of the material [43] such as metal, which is evaporated directly into a low-density gas; vapours diffuse rapidly from the hot source into the cold surrounding gas where they homogeneously nucleate to form nanoparticles. The particles

grow by coagulation, forming agglomerates that are collected by thermophoresis deposition on a stiff substrate [43].

Both Friedlander and Pui [44] categorized the evaporation condensation method into chemical and physical methods. The chemical vapour deposition method involves a chemical reaction, whereas the physical vapour deposition method uses heating and cooling of materials. Although the gaseous phase methods minimize the occurrence of organic impurities in the particles compared to the liquid phase, it requires the use of complicated vacuum equipment, which has the disadvantage of high costs and low productivity [44].

The chemical vapour deposition procedure can produce ultrafine particles of less than 1 μm by the chemical reaction occurring in the gaseous phase. The manufacture of nanoparticles of 10 to 100 nm is possible by careful control of the reaction. Performing the high-temperature chemical reaction in the chemical vapour deposition requires heat sources such as a chemical flame, a plasma process, a laser, or an electric furnace [44].

In the physical vapour deposition method, the solid material or liquid material is evaporated, and the resulting vapour is then cooled rapidly, yielding the desired nanoparticles. To achieve evaporation of the materials one can use an arc discharge method. The simple thermal decomposition method has been particularly fruitful in the production of metal oxide or other types of particles, and has been used extensively as a preferred synthetic method in the industrial world. Applications are reducing significant uncertainties in the global radiation balance, especially the poorly understood ‘indirect effects’ produced by nuclei that modify the

universal cloud cover and the hydrologic cycle. Other important applications are aerosols produced when hot vapours from pollution sources are injected into the atmosphere [44].

Although the gas evaporation method is a valuable laboratory tool, particle production rates are small [17]. Numerous efforts are focusing on continuous flow systems that operate at higher pressures with short residence times to increase rates of production of nanoparticles.

2.3 Particle Measurement

Particle measurement is typically specific to what is being measured and why. Different aerosols properties are classified into different aspects such as particle size, number, the shape of particles, mass, and surface area. Particle size is considered the most significant factor to characterize aerosol behaviour. On a nanoscale, both classical physics and quantum physics play roles in the interfacial behaviour of nanoaerosols. Some aspects have an impact on developing any measurement device [1].

Nanoparticle mass is one of these aspects, and because nanoparticles are small in mass, airborne nanoparticle analysis is complicated [45]. Some mass spectrometers have been designed to accelerate sample particles through a small orifice at flow rates of about $0.1\ l\ pm$ into a low pressure [46]. Most studies on nanometer diameter particles and health have focused on approximately isotropic primary particles, and agglomerates/aggregates of these particles. This raises additional concerns over the role of particle morphology when considering some complex nanostructured materials [9].

Studies have shown that despite the different particle compositions, sizes and morphologies, the aerosol surface area dose-response relationship appears to be remarkably similar for poorly

soluble, low toxicity particles [8]. Although monodisperse particles are used in describing particles with a narrow size distribution in nanoparticle manufacturing, most engineers deal with polydisperse aerosols. A polydisperse aerosol is a group of particles with different sizes suspended in the air. In the typical urban atmosphere, particle concentration can reach as high as $10^7 - 10^8 /cm^3$; their diameters can range from a few nanometers to around $100\ \mu m$ [47]. The size distribution of most polydisperse aerosol particles is lognormal. The majority of the products in these industries are primarily in powder form; therefore, particle size analysis is essential when producing powders as even small differences in size and shape as well as surface properties affect processability or performance and end product attributes. Consequently, powder dispersion is widely used to break up loose aggregate clusters to determine particle size distributions; this can be achieved using laser diffraction [9]. Real-time measurements of particle size distributions and particle structure are enabling technologies for the advancement of nanotechnology.

Research to improve our physical characterization capabilities includes rapid aerosol nanoparticle measurements, detection, characterization, and behaviour in the low nanometer, particle standards for size, concentration, morphology, and structure, charging behaviour and technology throughout the ultrafine and nanoparticle size regimes. In addition, distributed nanoparticle aerosol measurements are a fundamental component with primary parameter measurement, off-line morphological, structural, and chemical characterization of nanoparticles [44]. It is still a challenge to investigate ultra-fine particles because they have a small mass and high area distribution.

2.4 Knowledge Gap and Research Needed:

The process of particle charging and generating aerosols can be improved. In [1] it was attempted to develop a prototype that can charge fine particles. Even though the prototype gave good agreement compared to the SMPS, there were some investigations needed.

The corona charger is considered a more direct way of charging particles compared to the spark charger, which is mostly used to generate particles [8]. However, the need for a well characterized particle charging and generation device that is easy to manufacture is still essential.

Several limitations still existed with the prototype after the conclusion of the study, including particle losses due to the filtration in the corona charger, deposition in the system, and defocusing. The prototype was also unable to differentiate between particle shapes and agglomerates.

The corona charger can also be modified or substituted with other devices capable of producing high ion concentrations with low particle filtration. Consequently, further investigation is presented for the existence of the contamination that is presented at the corona charger by the needle because of the high electric field.

There are some limitations in developing a high voltage charger such as particle loss, which is caused by filtration by the high electric field. In addition, high voltage usage involves risks. Particle contamination that is caused by the needle material is a limitation for charging nanoparticle probes. Moreover, as the corona charger uses an electrometer to investigate the

charged nanoparticles, it is a challenge to distinguish between the agglomerate particles or the particle shape.

Different material could be used in the needle in the corona charger to limit the contamination of particles from the needle such as materials that have further resistance to oxidation and high conductivity in the electric field. Furthermore, a corona charger could be replaced by another device such as a UV charger or coupled with charging particle method before particles enter the corona charger.

Chapter 3. Theoretical Analyses and Discussion

The ideal charger for nanoparticles needs to have a high charging efficiency, a stable high ion concentration, low particle losses, lack of particle damage or contamination, and the use of different kinds of materials must be considered [11]. Passing the aerosol particles through the cloud of unipolar ions generated by electric discharge or bipolar ions generated by radioactive sources causes the aerosol particles to be charged. If the aerosol residence time is too high, then the particle loss is high due to Brownian diffusion into the walls. As a result, particle loss changes the measured number of airborne particles. Furthermore, the Brownian coagulation of particles varies the particle size distribution; the measured particle size distribution would differ from the actual distribution.

3.1 Corona Charger Assembling

The particle charging-detecting system is composed of six primary sections as in Figure 4: the aerosol generating section, the particle charging section, the pressure reducing section, the particle focusing section, the particle-detecting section, and the flow maintaining section. They are indicated in the following schematic drawing Figure 5 [1].

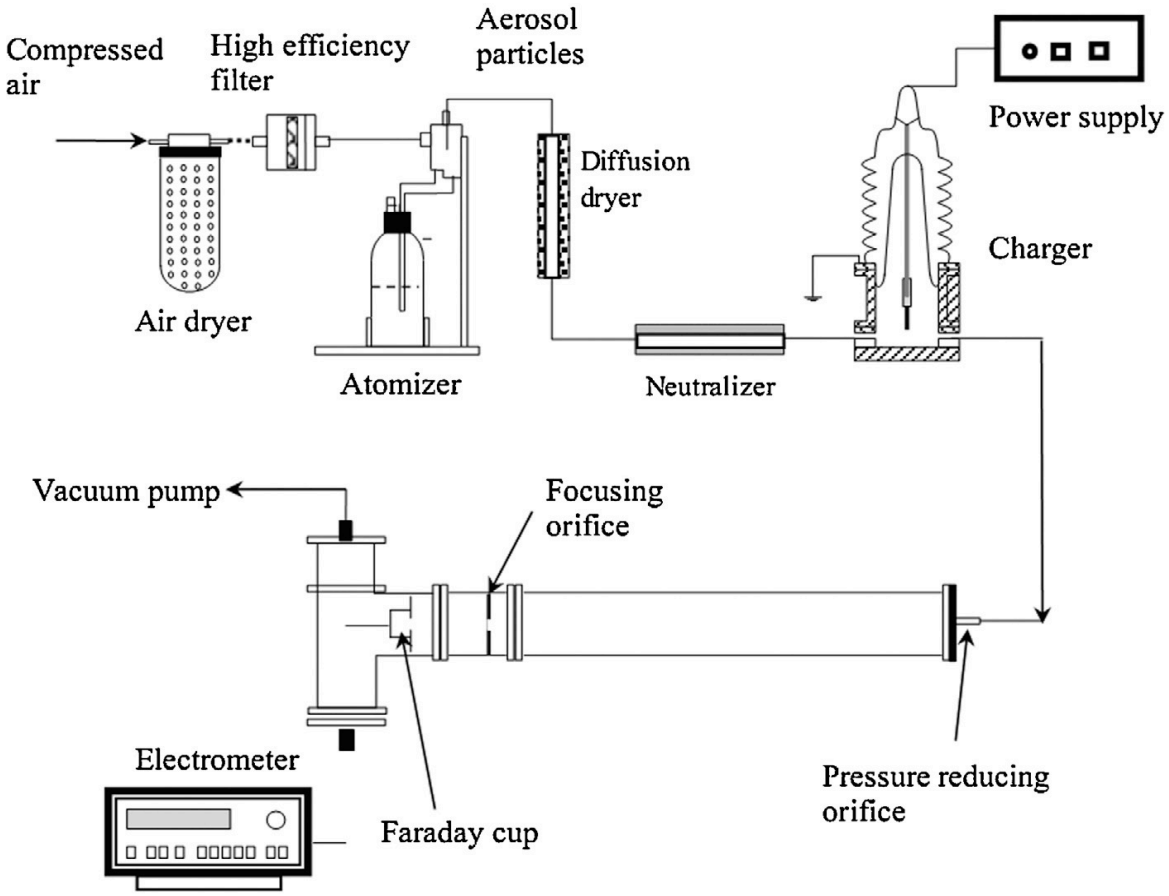

Figure 4: Experimental Setup for Evaluation of the Performance of the Prototype [48].

The corona charger investigated in this thesis is mainly connected to a high-voltage power supply (Glassman high voltage Model PS/EL30R01.5) to supply an electric potential in the range of $\pm 30\ kV$. Furthermore, the active electrode of the corona charger used is a gold needle with a sharp cone-shaped tip. The top of the needle was connected to a stainless-steel rod mounted into a ceramic isolator. The internal diameter of the bottom stainless steel plate was $37.5\ mm$. The distance between the plate and the needle tip (δ) was $12.7\ mm$, allowing air to pass through the corona while ions were polarizing the surrounding air molecules. Corona

discharge intensity can be regulated by adjusting the applied voltage or needle plate distance. The corona charge used is considered the simplest prototype due to it containing a single needle that can be adjusted in different prototypes.

In addition, a vacuum end is located inside the charging chamber. Flow rate is usually regulated by a vacuum pump at the end. Increasing the flow rate will increase ion diffusion since air flow will carry away more ions in the charging chamber.

Corona chargers are differentiated from other devices by maintaining a high concentration of unipolar ions, creating a high electric field intensity, and the ability to produce enough ions to charge particles located in the air flow.

The particle detecting system contains one pressure reducing section which includes one of the ten orifices and serves to control the downstream pressure and size of the focused particles, the focusing section, which focuses particles of the required size.

The flow analysis consists of a flowmeter and two pressure gauges coupled with a thermocouple. They are used to measure volume flow rate through the system, pressures before and after the focusing section as well as the temperature inside the tube, and the charge metering.

The charged particles that are deposited at the Faraday cup are measured, and an electrometer measures the electric current.

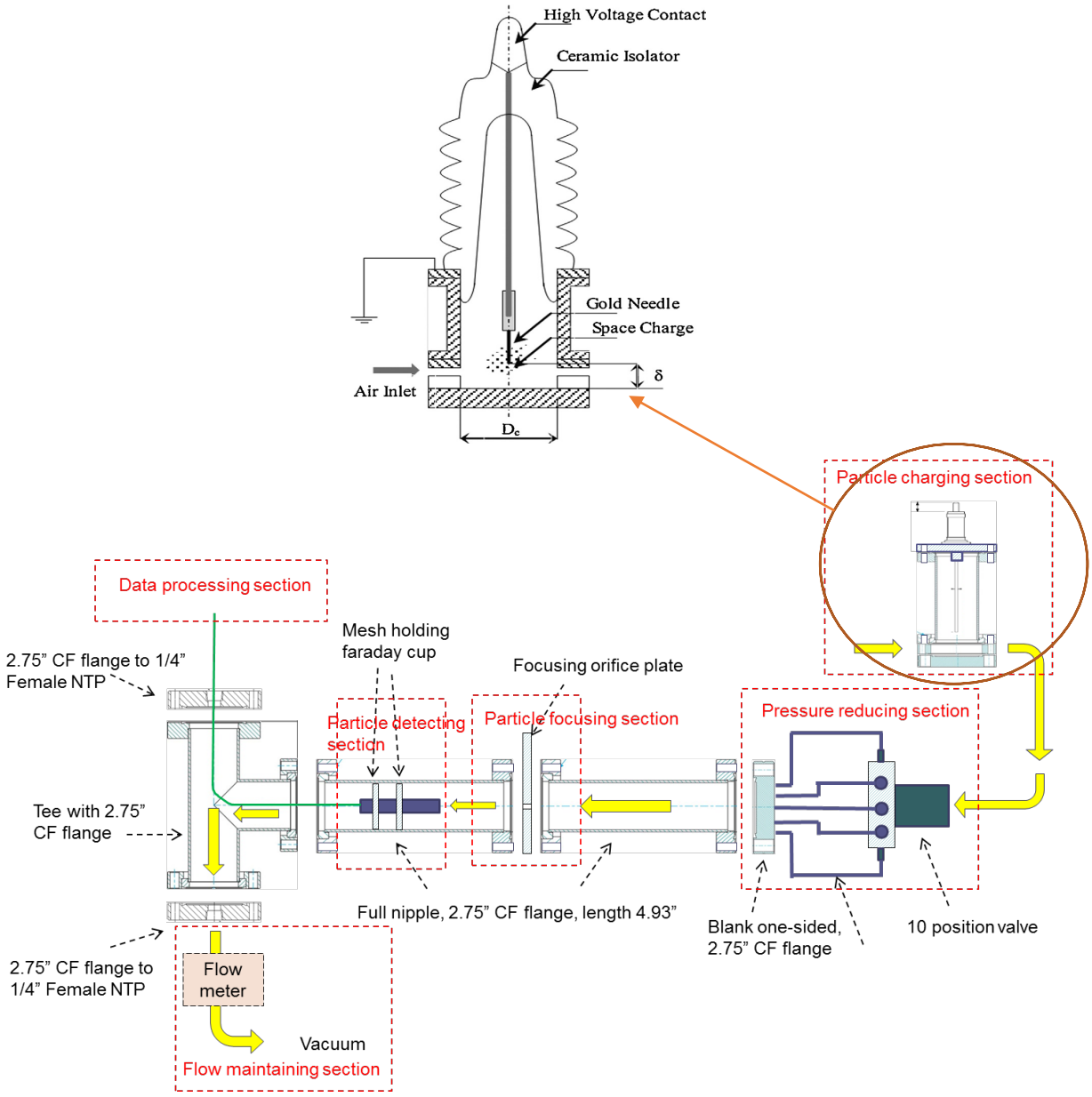

Figure 5: Schematic Diagram of the Home-Made Needle-Plate Corona Charger.

3.2 Theoretical Analysis

The corona charger produces a high electric field between electrodes, and gas flow, usually an inert gas, that carries the formed particles away from the production volume [49]. However,

the information on the complicated process of plasma formation to nanoparticle formation is limited. The corona charger, characterized by being friendly to the environment, does not need any solvent or chemical precursors, and does not contaminate its surroundings, which is a positive production principle. The ability to achieve particle purity and similarity to laser ablation, which can give a better understanding of spark ablation, is also a positive characteristic [49]. Usually, the corona charger consists of a power supply that results in plasma between two electrodes during X time.

Furthermore, needle to plate corona discharge was developed at first by [2] to generate ions in different types of gases. The corona charger ion generator consists of a sharp needle held at a high potential to produce the ions within nonconductive chambers. Afterward, there have been multiple developments of the corona charger throughout the years, depending on the purpose of the corona charger and the gas type. One of these corona charger developments was the homemade corona charger that was created by [1]. The idea of that corona charger was to charge the filtered air and produce ions and compare it to SMPS. However, there was an

interesting outcome, which were the gold nanoparticles that were collected and captured in the chemical composition as in Figure 6.

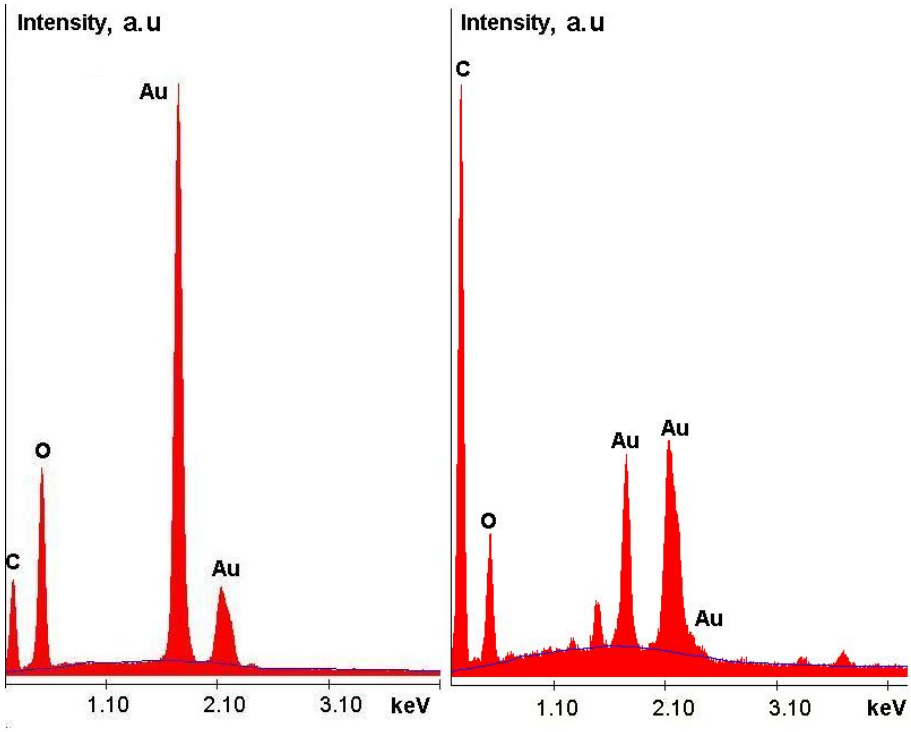

Figure 6: Chemical Composition of Particles Generated by Positive Corona Charger [1].

The gold particles were found due to a gold needle that was chosen as a reference material because of its very weak oxidation capability and high conductivity [50]. A sharp tip would have a focused electric field to allow for more charged particles as seen in Figure 7.

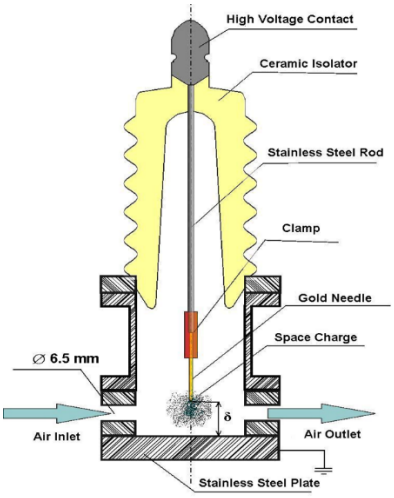

Figure 7: Corona Charger [1].

Furthermore, there are three explanations to account for the gold particles at the tip of the needle. One is chemical attack like oxidation corrosion [19].The second explanation is that it is the disintegration of the electrode because of the ions attacking the needle [19]. Finally, it could also be due to electrical erosion by the electric discharge [19]. However, this study will concentrate on calculating the erosion result from the electric discharge.

In addition, due to the existence of ions and electrons and gas molecules, plasmatic clouds are formed. This plasmatic region is considered a chemical reaction between the ions in the plasma and the electrons due to the collisions of these ions and electrons and molecules. In addition, at a high temperature, the gold needle evaporates and condensation appears in a chemical reaction that happens after the gold particles leave the needle as gold oxide to (Au_2O_3) [1]. However, the cooling period below the boiling point is relatively fast which causes the evaporation from the needle to decrease, and the aggregation to increase. As a result, it can be noticed that gold nanoparticles, due to these two mechanisms, require a thermodynamic

explanation. The evaporation mechanism comes from rapid heating of a small area on the electrodes, where the electrode material is heated to the boiling point. As a result of heat vapour, the gold material of the needle can be found [49]. The initial concentration is controlled by the voltage applied and the process gas flow rate.

Ultrafine particles were generated only when the supplied voltage is higher than a particular threshold value for the positive and negative corona chargers [1]. This phenomenon was explained by evaporation. The evaporation mechanism is mainly a thermal process depending on the amount of voltage applied and time. Voltage and time are the two parameters that control the amount of gold nanoparticle generation and size distribution. Evaporation of the gold nanoparticles needs a high voltage to reach the boiling point for gold material, realizing that evaporation and boiling are at a slightly similar degree in the sense that if one changes the physical water state from liquid to vapour, these are calculated in different ways. An investigation was run by [17] regarding the parameter affecting the electrode erosion, and found that the distance between electrode, type of air in the chambers, the capacitance between electrodes, and the material of the electrodes are all parameters that affect the amount of particles generated by the spark [17]. However, in Saprykina's thesis, most of the parameters are constant and the change was the voltage applied to the needle [1]. All things considered, the evaporation that happened at the needle tip required it to be heated up to the gold boiling point which is $Au = 2700C$ [1]. After reaching the temperature, voltage needs to continuously be added to the needle in order to increase heating to vaporize more gold particles or reduce the voltage to decrease the number of gold nanoparticles generated.

Calculation of the erosion can happen when the spark occurs [19]. As a result, the energy needed for the spark to evaporate by estimating Em the average value of the electric field between the needle tip and the stainless-steel plate is:

$$Em = \frac{V}{\delta} \quad 1$$

Where V is the voltage supplied to the corona charger, and δ is the distance between the gold needle and the bottom stainless steel plate.

Moreover, the electric field at the tip of the needle can be given by the axial field distribution which is

$$E(\xi) = \frac{2V}{ln\frac{4\delta}{r}} * \frac{1}{2\xi + r - \xi^2/\delta} \quad 2$$

Where ξ is the distance from the needle tip electric field and if much smaller from $\xi \ll \delta$, then $\xi = 0$ as exhibited in Figure 8.

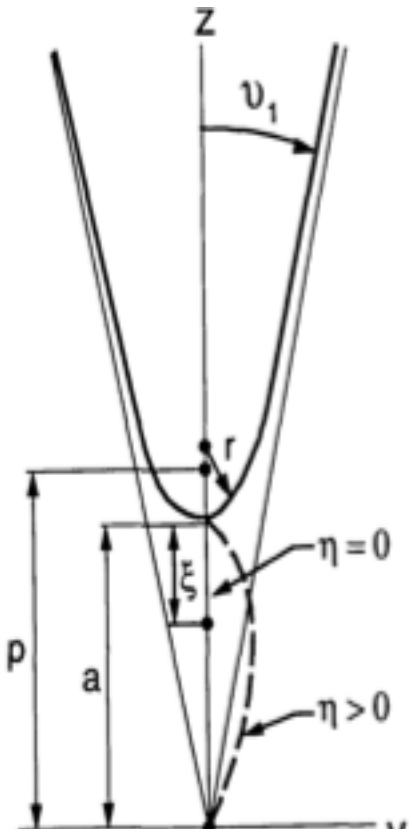

Figure 8: The Electric field at The Needle Tip [51]

So, $E\ (0)$ the field at the tip of the needle is given by:

$$E(0) = \frac{2V}{ln\frac{4\delta}{r}} * \frac{1}{r} \qquad 3$$

Where $E\ (0)\ (V/m)$ is the electric field,

$\delta(m)$ is the distance between the needle tip and the plate,

$V\ (v)$ is the voltage supply at the corona charger, and

$r(m)$ is the radius of the needle.

After finding the electric field, to find the amount of gold nanoparticles from [18] the energy required for evaporating the electrode material is given by

$$m(g) = \frac{\frac{1}{2}cV^2 - 4.2 * bT_b{}^4 - gk(T_b - T_s)}{\left[C_{ps}(T_m - T) + \nabla H_m + C_{pl} * (T_b - T_m) + H_v\right]} \quad 4$$

The first term is to present the effect spark energy depending on voltage and capacitance.

$$W = \frac{1}{2}c(F)V^2(V) \quad 5$$

C is the energy stored in a capacitor, and because we want to calculate electricity generated at the needle tip instead of calculating the voltage we can replace it by the electric field where:

$$c = \frac{K_A \varepsilon o A}{\delta} \quad 6$$

εo is the permanent permittivity of vacuum which is equal to $\varepsilon o = 8.85 * 10^{-12}(\frac{C^2}{N.m^2})$,

$A\ (m)$ is electrode area from the prototype for the plate and the needle, which is equal to the plate area plus the needle area so:

$A = (A1 + A2)/2 = (.0375 + .00025) = .03775\ m$, and δ is the space between the electrode, $K_A(\frac{jols}{sec} * \frac{1}{cm * C})$is air conductivity and it is = 1 [52]so the equation will be

$$c = \frac{\varepsilon o A}{\delta} \quad 7$$

Similarly, the voltage is calculated as the electric field multiplied with the distance between the needle and the tip,

$$V^2 = E^2\delta^2 \quad 8$$

So, W could change into

$$W = \frac{1}{2}cV^2 = \frac{1}{2}\varepsilon oA\delta E^2 \quad 9$$

The second aspect is the heat loss from the heat spot by radiation which is Tb while $b = A\sigma t$ σ is constant depending on the blackness of the bodies. t is time for energy transfer and A is the total area [19].

The third is under the heat transfer from the hot spot by conduction, in which k is the thermal conductivity and g is constant which is equal to $g = 2(\pi A)^{.5}t$, $k(\frac{jols}{sec} * \frac{1}{cm*C})$ is gold conductivity which is equal to 2.9.

The total energy Et has calculated the dissipation of energy process using three components. This is an estimate for evaporating the material, where cv^2 is the amount of energy given to the electrode, (bT) the losses of energy, and $gk(T_b - T_{GT})$ is radiation of energy.

The total mass m is equal to $m = \rho v$, where v is the total volume eroded from the needle of gold particles evaporated from the needle. As a result, equation 8 will become

$$v(cm^3) = \frac{2W - 4.2 * bT_b{}^4 - gk(T_b - T_s)}{\rho[C_{ps}(T_m - T) + \nabla H_m + C_{pl} * (T_b - T_m) + H_v]} \quad 10$$

All constants can be found in Table 2.

Table 2: Physical Properties of Gold.

Parameters	**Definitions**
Metal	Gold (Au)

Density $\boldsymbol{\rho}(\frac{g}{cm^3})$	19.3
Boiling point $T_b(K)$	2700C, 2972 °K
Melting point T_m(K)	1064C, 1337 °K
$\boldsymbol{T_s}$	Steady temperature 20℃
Thermal conductivity $k(jols/sec *$ $\frac{1}{cm*C}$)	2.9
Specific heat, $s(\frac{jouls}{gram*C})$	0.13
Molecular weight (g/mol)	197
Latent heat (j/g)	1.7
$\boldsymbol{b}$	$2 * 10^{-20} Cal\ per(K)^4$ Constant [19]
$\boldsymbol{g}$	$.95 * 10^{-8} cm * sec$ Constant [19]
$\boldsymbol{H_v}$	Enthalpy of evaporation$(gram/J)$)
$\boldsymbol{H_m}$	Enthalpy of melting$(gram/J)$).
$\boldsymbol{C_{pl}}$	The energy needed to heat the liquid to boiling point $(J/gram * (°K))$
$\boldsymbol{C_{ps}}$	Average heat capacitance for solid$(J/$ $gram * (°K))$

3.3 Experimental Part

Saprykina provided a concentration and size distribution for the filtered air at voltages $12000\ V$ and $17000\ V$ as in Table 6 and Table 7 [1].

There was a flow analysis that used an electrometer Faraday cup to analyze and count the particles charged from the corona charger.

The equations used to calculate the distribution size are

$$dp = \sqrt{\left(\frac{1.657\mu}{\rho\sqrt{(2M}/\pi RT\ )}\right)^2} + \left(\frac{18MdStK}{\rho Vf}\right) - \frac{1.657M}{\rho\sqrt{\frac{2M}{\pi RT}}} \quad 11$$

$$N = \frac{I}{\frac{dpkTQ}{2eK} ln\left(1+\left(\frac{dpkec\pi e^2 cN_i t}{2Kt}\right)\right)} \quad 12$$

All parameters are found in Table 3.

Table 3: Parameters

Parameters	**Meaning**
$\boldsymbol{\mu}$	Dynamic gas viscosity, which is a constant and a function of temperature equal to $1{,}83E-5\ \ Kg/(m.s)$
$\boldsymbol{\rho}$	Density of air $\frac{kg}{m^3}$
$\boldsymbol{M}$	Molar mass of the gas $\frac{kg}{mol}$
$\boldsymbol{R}$	Universal gas constant $\frac{J}{K.mol}$
$\boldsymbol{T}$	Temperature $°K$

$\boldsymbol{StK}$	Stokes number is defining the size of the focused particles taken as 1 [1]
$\boldsymbol{Vf}$	Gas velocity m/s
$\boldsymbol{I}$	Ion Current A
$\boldsymbol{Q}$	Volume flow rate 1.4 lpm m^3/s
$\boldsymbol{e}$	Elementary charge$C$
$\boldsymbol{c}$	Constant determent by DMA
$\boldsymbol{t}$	Time s

From the concentration of the particle and dp size distribution, it was possible to calculate the total mass of the filtered air by some simple calculation:

$$dp(nm) = \frac{dp}{10^{-9}}(m) \quad 13$$

Then

$$dp - v(m) = (\pi * \frac{(dp^3)}{6}) * 10\text{^}6(cm^3) \quad 14$$

The number of particles can be calculated

$$N(\#) = \frac{C(\#/cm^3)*1000}{dp(cm^3)*1.85} \quad 15$$

The total volume for the particles

$$v_t = C * dp(cm^3) \quad (16)$$

The volume with respect to the flow rate

$$v_{t/q} = (v_t * (1.4 * 10\text{^}3))/60 \quad (17)$$

As a result, it is now possible to calculate the total mass for the filtered air and gold particles

$$m_t(g) = (v_{\frac{t}{q}}(Cm^3) * 11.3))/100 \quad (18)$$

Because gold tends to oxidize under the high electric field and high temperature the density of (Au_3O_2) gold oxide was used.

3.4 Ozone Composition

Filtered air is introduced to the corona charger chamber that contains oxygen. As a result, the ozone generated under the needle includes positive and negative ions, and particles. There are two reactions happening: the ozone radical ionic reaction as in Equation 19, and ozone being generated by free radical reaction as in Equation 20.

$$O_2 + 2e \rightarrow O_2^+ + 2e$$

$$\rightarrow O^+ + O + 2e$$

$$\rightarrow O + O + e$$

$$\rightarrow O^- + O \quad (19)$$

$$2M + O_2 + O \rightarrow M + O_3 \quad (20)$$

M could be O_2 *or* N_2 [53]. However, in this case, M refers to Au as the gold nanoparticles enter the reaction zone. Therefore, it was assumed that Au_2O_3 was formed.

3.5 Results and Discussion

In seeking to investigate and analyze the characteristics of the mass of both the gold particles and the total amount of particles in the experiment, a figure was drawn to show the difference. The gold nanoparticles were investigated in both negative and positive electric fields. In the experiment that was conducted, it was proven that there are gold nanoparticles generated due to the high electric field that was applied to the needle at $(11 - 12KV)$ [1]. In the chemical composition that was tested in [1] by Scanning Electron Microscopy (SEM) and Transmission Electron Microscopy, the existence of gold nanoparticles was found at the positive electric field between $(E\ (0)\ = 16559 - 18065)$. The gold particles exist due to the gold needle that was eroded by the high electric field applied to the needle. Another factor that can affect the gold particles is the distance between the needle and the plate in the corona charger. However, in the experiment, the distance was constant: equal $12,7\ mm$. As a result, the variable that controls the mass of gold particles is the amount of voltage applied.

Table 4 shows the total mass that was calculated from the experiment. From the size distribution and the particle concentration the total mass for the total particles was calculated. There were a small amount of the total particles which contained oxygen, carbon and gold particles. The amount of the mass increased suddenly when the spark happened at 12KV. Then the amount of the total mass decreased after the discharge accrued, and that might have caused the gold particles to sputter from the needle due to the spark.

Table 4: Total Mass of Particles in Positive Corona Charger.

Voltage (KV)	**Mass (g)**
0	1.73E-13
2	1.83E-13
4	1.76E-14
6	2.39E-15
8	1.10E-15
10	8.65E-16
12	8.95E-10
13	4.20E-16

It is notable that there occurred a sudden increase in the mass amount at $12\ KV$ when the spark increased from Figure 9. This escalation proves that the amount of gold nanoparticles mostly exists when the spark happened due to the energy release at the tip of the needle.

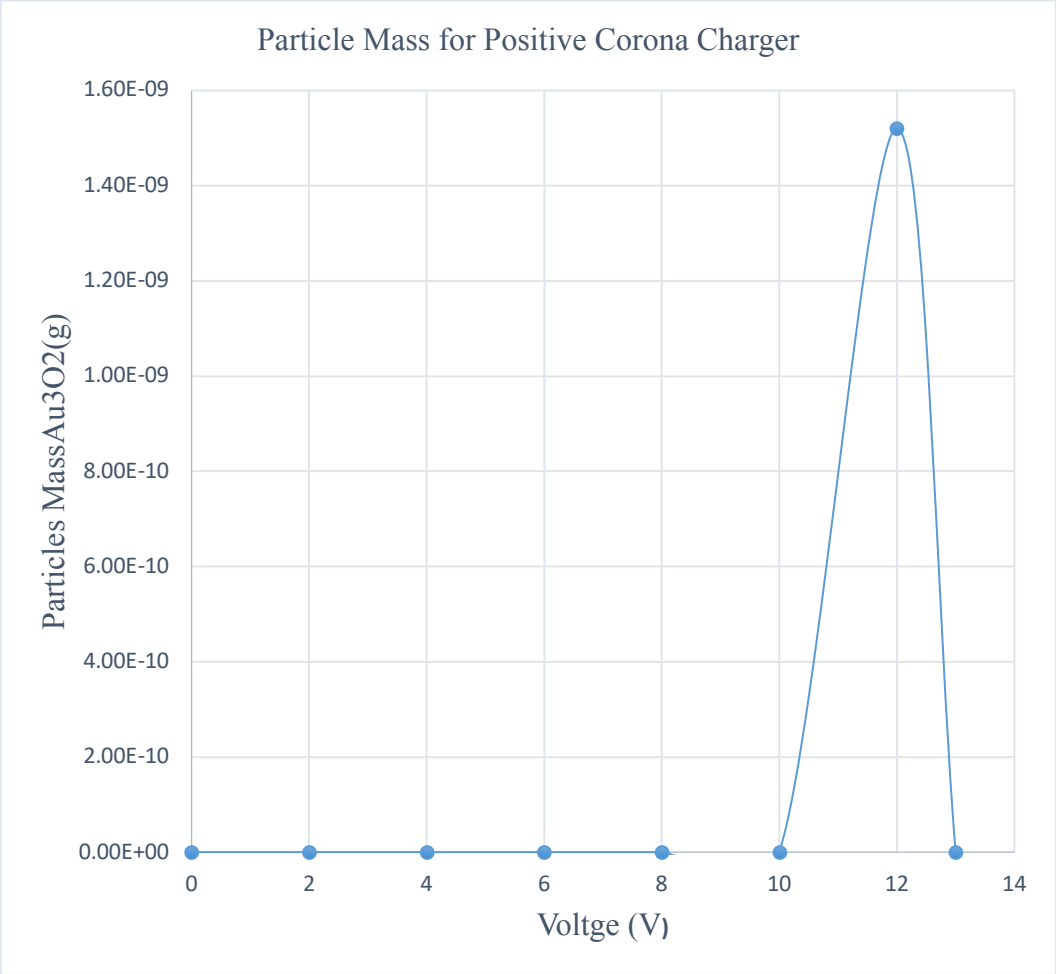

Figure 9: Total Mass of Particles in Positive Corona Charger.

In the current study, the amount of gold particles was calculated when the spark occurred at 12 KV for positive and 17KV for negative as it is indicated in

Table **5**. As the voltage was applied, the gold particles started to evaporate from the needle due to the electric field. When the spark occurred, the amount of energy released affected the material of the anode, releasing a higher amount of the particles at the tip of the needle.

In Table 5, the electric field at the tip of the needle was calculated, then the volume and mass of the gold was calculated in both positive and negative charge. Then the oxidized gold mass was calculated under the assumption that gold particles are oxidized due to the electric field and the plasma that contained filtered air. It is notable that the amount of mass particles was higher for negative than for positive. Negative voltage has a high intensity that cues a higher amount of mass in the negative voltage.

Table 5: Theoretical Total Mass Erosion at the Spark.

Charge	**V, V**	$E(0), (\frac{V}{m})$	$vg(cm\text{^}3)$	**Mass** (Au)	**Mole** (Au)	**Mass**(Au_2O_3)
Positive	12500	1.88E+07	2.39E-05	4.62E-11	2.35E-13	5.19E-11
negative	17000	2.56E+07	5.55E-05	1.07E-10	5.44E-13	1.20E-10

Subsequently, the amount of erosion for gold nanoparticles in negative and positive voltage can be found in Figure 10. For the negative charge, the amount of mass at the spark that happened at $(17KV)$ is $(1.20 * 10^{-10}\text{g})$. For the positive charge, the amount of mass at the spark that happened at $(12KV)$ is $(5.95 * 10^{-10}\text{g})$. The difference in the total mass for the charger is cause by the intensity of the negative charge. In addition, the intensity of the negative charge can cause bigger particles [1] to escape from the needle, which leads to higher mass.

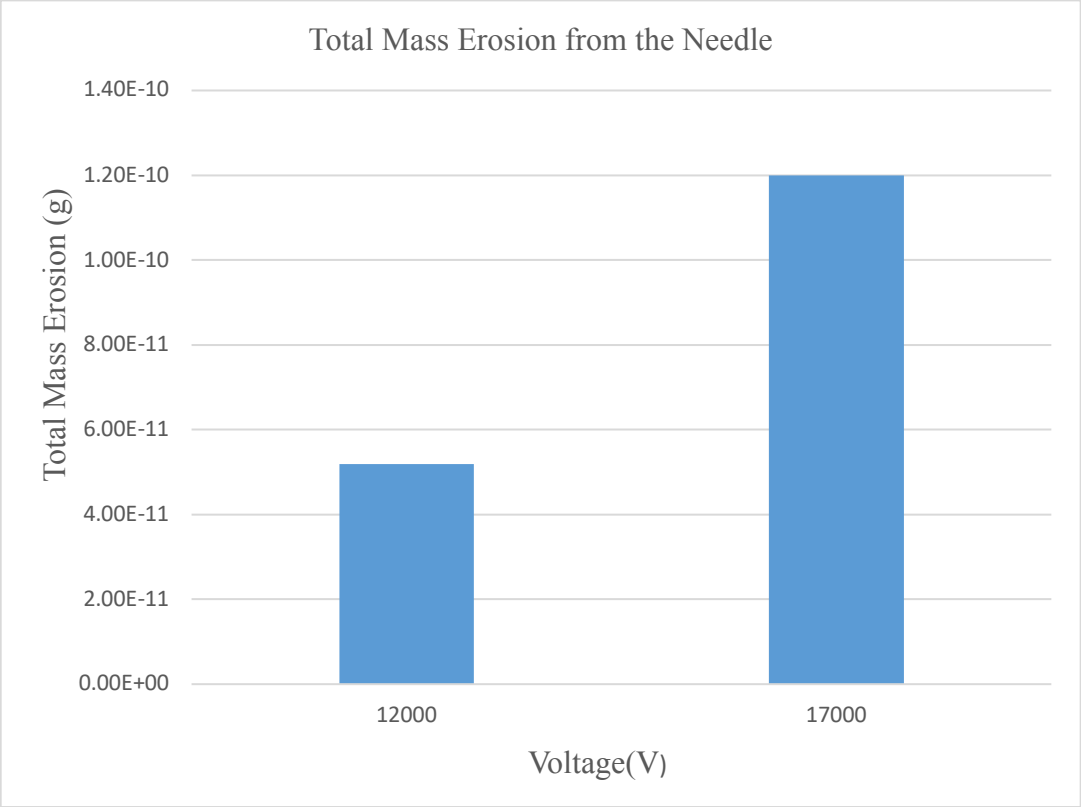

Figure 10: Total Mass Erosion from the Needle.

A comparison between the masses of particles generated in the corona charger was presented in Figure 11. It is clear that the production of the total mass particles for negative is higher than it is in positive charge. Similarly, the oxide gold particles also agreed with the total mass of particles in the corona charger. Accordingly, the negative charge had slightly higher oxide gold particles than the positive voltage.

Furthermore, the mass of the oxide gold particles in the positive charge was 5.7% from the total mass of the total particles that were in the experiment. It could be explained that the experiment was higher due to the carbon existence and the oxygen that was not oxidised with the gold particles.

As well as for negative particles charged, the gold mass was considered 3.2 % of the total mass of the particles which was ($3.64 * 10^{-9}$g). These results were expected because the negative charge has higher strength than the positive. Therefore, the intensity of the electric field in the spark affects the mass of gold nanoparticles.

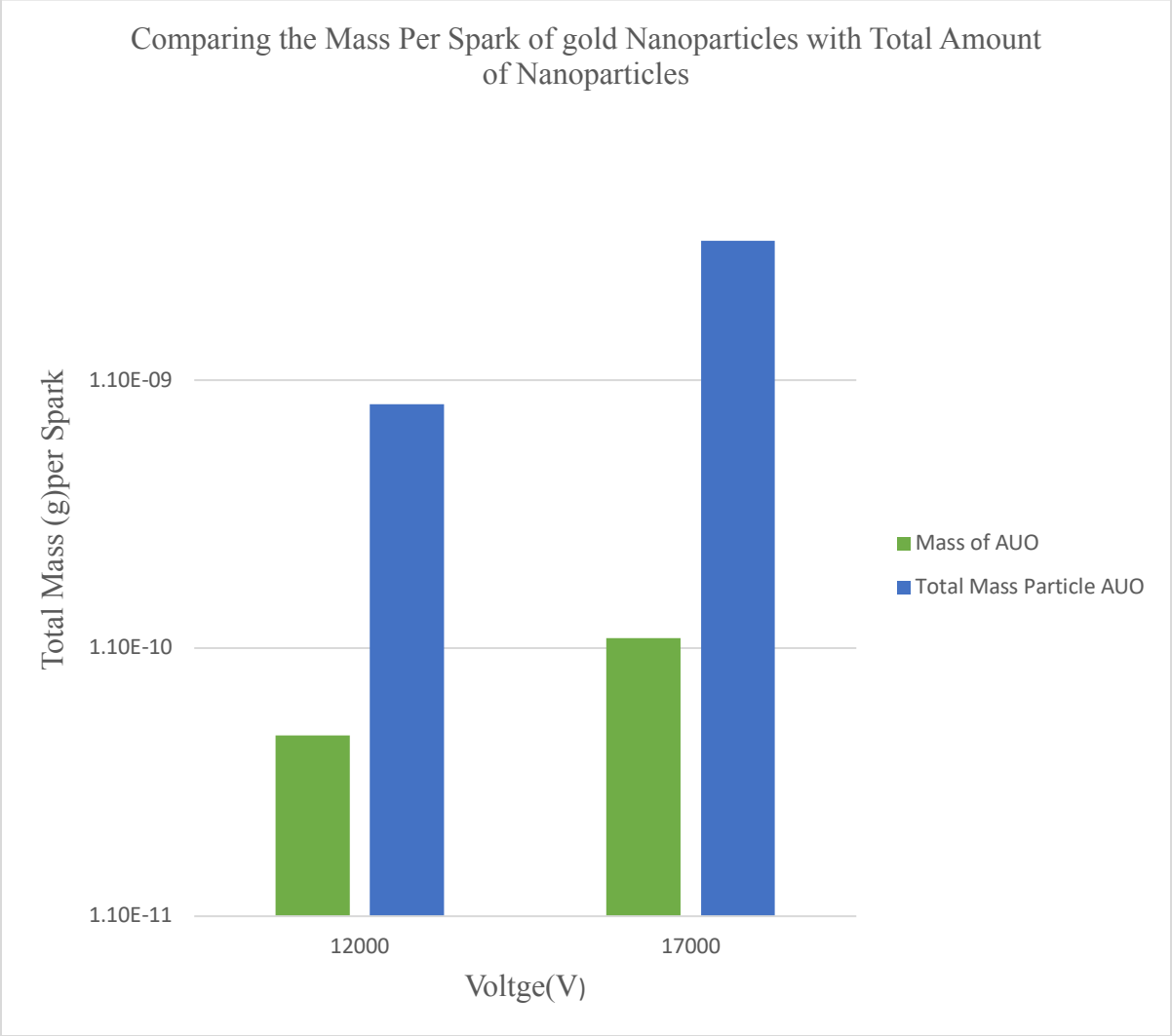

Figure 11: Comparing the Mass per Spark of gold Nanoparticles with Total Amount of Nanoparticles.

Furthermore, the difference between the experimental results and the theoretical results may be explained by other aspects affecting the erosion of the needle such as the availability of other particles like carbon from the plate and oxygen. Another explanation is that gold particles were generated before the spark occurred and that might be the cause behind the difference in the result.

Some studies focused on the erosion of the metal in spark generation, and it was found that gold and tungsten are materials that are difficult to erode because they are noble metals [20]. In addition, they do not oxidise or corrode. However, in it was found that tungsten has a higher tolerance in the high electric field than gold [20]. On the other hand, materials such as copper, platinum, and nickel, have a higher erosion rate, which is an advantage for deposition purposes [19]. After the gold nanoparticles leave the needle, they tend to oxidize in the presence of a strong electric field in the corona charger [1]. In this case, the high electric field caused a plasmatic cloud to form under the needle. This cloud of positive and negative ions and electrons tended to evaporate and frequently condense as long as the electric field was added. Unexpectedly, the total mass in the experiment increased while the number of the particles remained constant between $12000 - 20000$[1], which means that the particle size increased while the electric field increased. As a result, it is expected that gold particle mass will increase with multiple sparks in the corona charger.

After the gold nanoparticles leave the needle, they tends to oxidize in the presence of a strong electric field in the corona charger. As a result, gold (III) oxide (Au_2O_3)is formed [1]. There was no presence of iron from the stainless-steel plate, either because it was grounded or

because the spark energy did not produce enough heat on the plate that cues evaporation of the iron particles.

Additionally, the calculation eliminates the effect of a chemical reaction to calculate the mass of gold. However, after calculating the total mass of gold it was possible to find the oxidized gold under the assumption that all gold particles oxidize under the high electric field and the high temperature. As a result, the results conducted were based on thermal calculations.

Chapter 4. Conclusions and Recommendations

4.1 Conclusions

Theoretical analysis and experimental evaluation showed that it is feasible to measure the mass of airborne submicron particles by particle charge measurement and the mass of gold particles. Charging improved the prototype and eliminated any needle erosion. Overall, the gold particle mass was calculated and compared with experimental findings. In addition, gold nanoparticles were generated, considering both positive and negative electric fields. As a result, the amount of gold nanoparticles was investigated when a spark was released. Also, the mass of gold nanoparticles is higher in the negative electric field than it is in the positive electric field.

Corona chargers are air ionizers that were used to charge and filtrate the air. Accordingly, gold nanoparticles were considered a contamination of the results; however, the process can be utilized in other applications. By varying the distance between the corona tip and the grounded substrate and the voltage applied to the tip, the intensity of the corona discharge can be controlled, resulting in generation of particles with different diameters [20].

According to the experimental results, the gold nanoparticles were present before the spark, even though the spark generated more gold particles from the needle. As a result, there were gold nanoparticles in the corona charger, but they were less than the total amount of particle measured by electrometer.

During the charger method with the corona charger, the breakdown limit of the charger should be avoided. Therefore, there is still a need to improve the performance of existing technologies or to develop alternative ones for the measurement of particle number concentration distribution [54]. Despite the errors in the experimental parts, the prototype could measure particles in the range of $40\ nm$ to $300\ nm$ in good agreement with $SMPS$. More research shall be done using the alternative corona charger with different types of needles.

4.1.1 Limitations

A drawback for the modeling section was that it could calculate the amount of total mass only when the spark happened and neglected any particles generated before the spark. As a result, the corona charger that was used had one spark to estimate the total mass and that was what may have caused the difference between the experimental data and the modeling data. Furthermore, there were carbon particles that were not possible to calculate because the plate was grounded and did not have an energy source to calculate by the theoretical model. Another downside was that the negative total mass for the experiment was limited due to the negative charge intensity and there was no data after the voltage exceeded $17\ KV$. However, it

can be seen that there is a gradual increase in the total mass for negative charge until it reaches a maximum of 17 KV as shown in Figure 12.

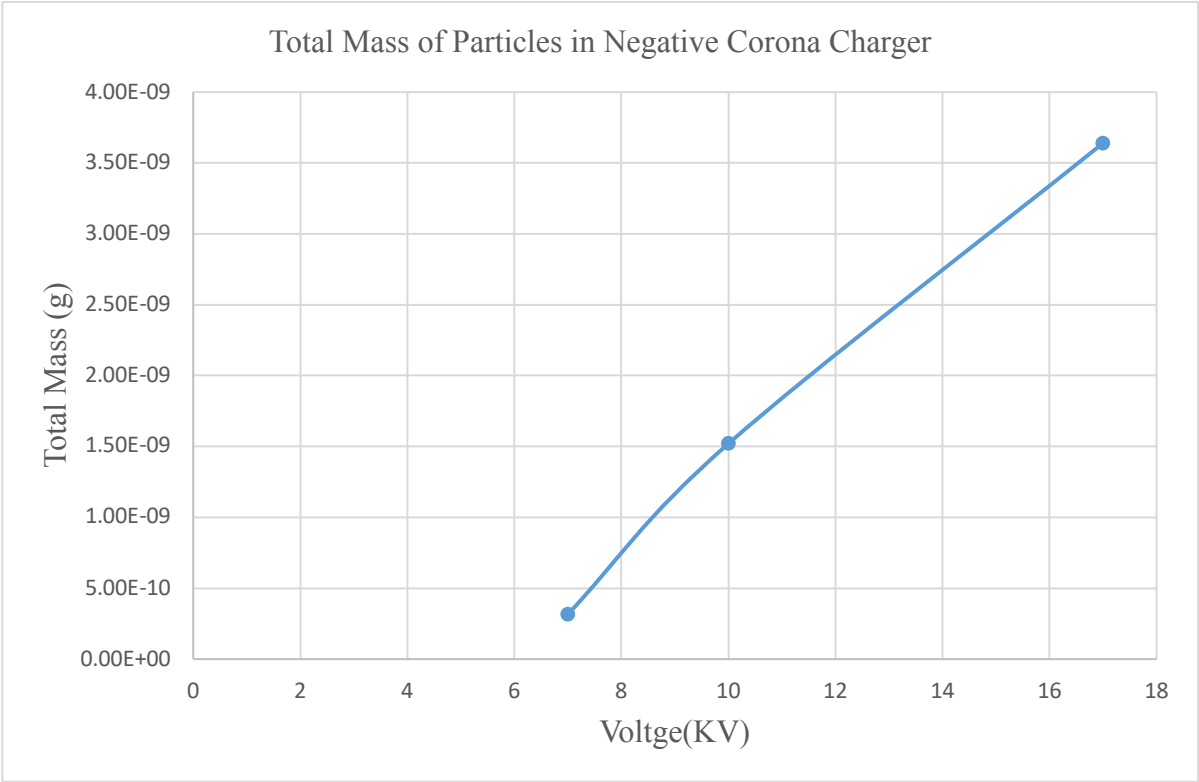

Figure 12: Total Mass of Particles in Negative Corona Charger.

4.2 Recommendations

Measuring particle size distribution in particles below 40 nm with a corona charger could be reached through the use of a strong pump. Thus, a lower pressure can be achieved using a different material for the needle to eliminate erosion, with materials such as tungsten, graphene, or mixed metal, which will have a better tolerance for the high voltage. The use of a tungsten needle may reduce the number of contamination particles.

To improve the corona charging efficiency without producing any particles from the needle will require changing the needle type or charging the particles. Charging the particles before entering the chamber by injecting ions and mixing them with the particles could prevent precipitation in the needle contamination.

Although the current homemade corona charger served its purpose for particle charging, it did generate particles from the gold needle. In addition, it was shown that corona chargers generate nanoparticles at higher voltages. As a result, it might be better to use the homemade corona charger to generate and deposit material that depends on the needle material used.

References

[1] A. Saprykina, *Airborne Nanoparticle Sizing by Aerodynamic Particle Focusing and Corona Charging.* Library and Archives Canada= Bibliothèque et Archives Canada, 2010.

[2] K. Whitby, "Generator for producing high concentrations of small ions," *Rev. Sci. Instrum.,* vol. 32, *(12),* pp. 1351-1355, 1961.

[3] H. Paur *et al*, "In-vitro cell exposure studies for the assessment of nanoparticle toxicity in the lung—A dialog between aerosol science and biology," *J. Aerosol Sci.,* vol. 42, *(10),* pp. 668-692, 2011.

[4] G. Oberdorster, E. Oberdorster and J. Oberdorster, "Nanotoxicology: an emerging discipline evolving from studies of ultrafine particles," *Environ. Health Perspect.,* vol. 113, *(7),* pp. 823-839, Jul, 2005.

[5] R. Givehchi and Z. Tan, "An overview of airborne nanoparticle filtration and thermal rebound theory," *Aerosol and Air Quality Research,* vol. 14, *(1),* pp. 45-63, 2014.

[6] Z. Tan, *Air Pollution and Greenhouse Gases: From Basic Concepts to Engineering Applications for Air Emission Control.* Springer, 2014.

[7] C. M. Welch and R. G. Compton, "The use of nanoparticles in electroanalysis: a review," *Analytical and Bioanalytical Chemistry,* vol. 384, *(3),* pp. 601-619, 2006.

[8] B. Tan, "Laboratory Evaluation of Low to Medium Cost Particle Sensors," 2017.

[9] G. Calvert, M. Ghadiri and R. Tweedie, "Aerodynamic dispersion of cohesive powders: a review of understanding and technology," *Advanced Powder Technology,* vol. 20, *(1),* pp. 4-16, 2009.

[10] B. Grob, H. Burtscher and R. Niessner, "Charging of ultra-fine aerosol particles by an ozone-free indirect uv photo-charger," *Aerosol Science and Technology,* vol. 47, *(12),* pp. 1325-1333, 2013.

[11] P. Intra and N. Tippayawong, "An overview of unipolar charger developments for nanoparticle charging," 2011.

[12] J. H. Turner *et al*, "Sizing and Costing of Electrostatic Precipitators: Part I. Sizing Considerations," *Japca,* vol. 38, *(4),* pp. 458-471, 1988.

[13] H. C. Oh *et al*, "Synthesis of titania nanoparticles via spark discharge method using air as a carrier," in *Materials Science Forum,* 2007, pp. 143-146.

[14] C. S. Kim *et al*, "Filtration efficiency of a fibrous filter for nanoparticles," *Journal of Nanoparticle Research,* vol. 8, *(2),* pp. 215-221, 2006.

[15] A. Yehia and A. Mizuno, "Expectation of ozone generation in alternating current corona discharges," *Phys Plasmas,* vol. 19, *(3),* pp. 033513, 2012.

[16] C. Kimblin, "Erosion and ionization in the cathode spot regions of vacuum arcs," *J. Appl. Phys.,* vol. 44, *(7),* pp. 3074-3081, 1973.

[17] N. S. Tabrizi *et al*, "Generation of nanoparticles by spark discharge," *Journal of Nanoparticle Research,* vol. 11, *(2),* pp. 315, 2009.

[18] F. L. Jones, "Electrode erosion by spark discharges," *British Journal of Applied Physics,* vol. 1, *(3),* pp. 60, 1950.

[19] F. Llewellyn-Jones, "The mechanism of electrode erosion in electrical discharges," *Platinum Metals Review,* vol. 7, *(2),* pp. 58-65, 1963.

[20] A. Biris *et al*, "Corona generation and deposition of metal nanoparticles on conductive surfaces and their effects on the substrate surface texture and chemistry," *Particul. Sci. Technol.,* vol. 22, *(4),* pp. 405-416, 2004.

[21] P. Intra and N. Tippayawong, "Progress in unipolar corona discharger designs for airborne particle charging: A literature review," *J. Electrostatics,* vol. 67, *(4),* pp. 605-615, 2009.

[22] L. Li, "Electrical and magnetic separation of particles," 2010.

[23] J. Jiang, M. Lee and P. Biswas, "Model for nanoparticle charging by diffusion, direct photoionization, and thermionization mechanisms," *J. Electrostatics,* vol. 65, *(4),* pp. 209-220, 2007.

[24] G. Hewitt, "The charging of small particles for electrostatic precipitation," *Transactions of the American Institute of Electrical Engineers, Part I: Communication and Electronics,* vol. 76, *(3),* pp. 300-306, 1957.

[25] P. Intra and N. Tippayawong, "Design and evaluation of a high concentration, high penetration unipolar corona ionizer for electrostatic discharge and aerosol charging," *J.Electr.Eng.Technol,* vol. 8, *(5),* 2013.

[26] A. Hernandez-Sierra, F. Alguacil and M. Alonso, "Unipolar charging of nanometer aerosol particles in a corona ionizer," *J. Aerosol Sci.,* vol. 34, *(6),* pp. 733-745, 2003.

[27] C. Qi, D. Chen and D. Y. Pui, "Experimental study of a new corona-based unipolar aerosol charger," *J. Aerosol Sci.,* vol. 38, *(7),* pp. 775-792, 2007.

[28] S. Kimoto *et al*, "Aerosol charge neutralization by a mixing-type bipolar charger using corona discharge at high pressure," *Aerosol Science and Technology,* vol. 43, *(9),* pp. 872-880, 2009.

[29] Z. Tan and A. S. Wexler, "Fine particle counting with aerodynamic particle focusing and corona charging," *Atmos. Environ.,* vol. 41, *(25),* pp. 5271-5279, 2007.

[30] A. Medved *et al*, "A new corona-based charger for aerosol particles," *J. Aerosol Sci.,* vol. 31, pp. 616-617, 2000.

[31] C. Huang and M. Alonso, "Nanoparticle electrostatic loss within corona needle charger during particle-charging process," *Journal of Nanoparticle Research,* vol. 13, *(1),* pp. 175-184, 2011.

[32] D. Pui, S. Fruin and P. McMurry, "Unipolar diffusion charging of ultrafine aerosols," *Aerosol Science and Technology,* vol. 8, *(2),* pp. 173-187, 1988.

[33] M. Adachi, Y. Kousaka and K. Okuyama, "Unipolar and bipolar diffusion charging of ultrafine aerosol particles," *J. Aerosol Sci.,* vol. 16, *(2),* pp. 109-123, 1985.

[34] M. Alonso, A. Hernandez-Sierra and F. J. Alguacil, "Diffusion charging of aerosol nanoparticles with an excess of bipoloar ions," *Journal of Physics A: Mathematical and General,* vol. 35, *(30),* pp. 6271, 2002.

[35] G. A. Lozano *et al*, "Enhanced volumetric hydrogen density in sodium alanate by compaction," *J. Power Sources,* vol. 196, *(22),* pp. 9254-9259, 2011.

[36] A. Schmidt-Ott, P. Schurtenberger and H. Siegmann, "Enormous yield of photoelectrons from small particles," *Phys. Rev. Lett.,* vol. 45, *(15),* pp. 1284, 1980.

[37] M. Alonso and F. Alguacil, "Particle size distribution modification during and after electrical charging: Comparison between a corona ionizer and a radioactive neutralizer," *Aerosol and Air Quality Research,* vol. 8, *(4),* pp. 366-380, 2008.

[38] Y. Kousaka *et al*, "Measurement of electric charge of aerosol particles generated by various methods." *J. Chem. Eng. Japan,* vol. 14, *(1),* pp. 54-58, 1981.

[39] F. J. Romay and D. Y. Pui, "On the combination coefficient of positive ions with ultrafine neutral particles in the transition and free-molecule regimes," *Aerosol Science and Technology,* vol. 17, *(2),* pp. 134-147, 1992.

[40] B. Han *et al*, "Unipolar charging of nanosized aerosol particles using soft X-ray photoionization," *Aerosol. Sci. Technol.,* vol. 37, *(4),* pp. 330-341, 2003.

[41] E. Manirakiza *et al*, "High-efficiency unipolar charger for sub-10 nm aerosol particles using surface-discharge microplasma with a voltage of sinc function," *Aerosol Science and Technology,* vol. 47, *(1),* pp. 60-68, 2013.

[42] S. Kala, R. Theissmann and F. E. Kruis, "Generation of AuGe nanocomposites by co-sparking technique and their photoluminescence properties," *Journal of Nanoparticle Research,* vol. 15, *(9),* pp. 1963, 2013.

[43] H. Masuda, K. Higashitani and H. Yoshida, *Powder Technology: Fundamentals of Particles, Powder Beds, and Particle Generation.* CRC Press, 2006.

[44] S. K. Friedlander and D. Y. Pui, "Emerging issues in nanoparticle aerosol science and technology," *Journal of Nanoparticle Research,* vol. 6, *(2),* pp. 313-320, 2004.

[45] C. A. Zordan, M. R. Pennington and M. V. Johnston, "Elemental composition of nanoparticles with the nano aerosol mass spectrometer," *Anal. Chem.,* vol. 82, *(19),* pp. 8034-8038, 2010.

[46] P. H. McMurry *et al*, "Sampling nanoparticles for chemical analysis by low resolution electrical mobility classification," *Environ. Sci. Technol.,* vol. 43, *(13),* pp. 4653-4658, 2009.

[47] Z. Tan, R. Givehchi and A. Saprykina, "Submicron particle sizing by aerodynamic dynamic focusing and electrical charge measurement," *Particuology,* vol. 18, pp. 105-111, 2015.

[48] Z. Tan, R. Givehchi and A. Saprykina, "Submicron particle sizing by aerodynamic dynamic focusing and electrical charge measurement," *Particuology,* vol. 18, pp. 105-111, 2015.

[49] T. Pfeiffer, J. Feng and A. Schmidt-Ott, "New developments in spark production of nanoparticles," *Advanced Powder Technology,* vol. 25, *(1),* pp. 56-70, 2014.

[50] N. E. Jewell-Larsen *et al*, "Modeling of corona-induced electrohydrodynamic flow with COMSOL multiphysics," in *Proc. ESA Annual Meeting on Electrostatics,* 2008, .

[51] B. Florkowska and R. Wlodek, "Pulse height analysis of partial discharges in air," *IEEE Transactions on Electrical Insulation,* vol. 28, *(6),* pp. 932-940, 1993.

[52] R. Wolfson, *Essential University Physics.* Addison-Wesley, 2015.

[53] J. Chang, P. A. Lawless and T. Yamamoto, "Corona discharge processes," *IEEE Trans. Plasma Sci.,* vol. 19, *(6),* pp. 1152-1166, 1991.

[54] N. Sabbagh-Kupelwieser *et al*, "Comprehensive physical and chemical characterization of urban aerosols in vienna, austria," in *The 7 Th Asian Aerosol Conference,* 2011, pp. 507.

Appendix

Table 6: Experimental Result for the Total Amount of particles in Positive Corona Charger.

	$U = 12kV$			
$dp\ (nm)$	$C, \#/cm\text{^}3$	$dp - v, cm\text{^}3$	$Volume/Q$	$Mass$
7.1	0	1.87402E-19	0	0
7.37	0	2.09605E-19	0	0
7.64	0	2.33496E-19	0	0
7.91	0	2.59136E-19	0	0
8.2	0	2.88696E-19	0	0
8.51	0	3.22691E-19	0	0
8.82	0	3.59256E-19	0	0
9.14	0	3.99795E-19	0	0
9.47	0	4.44681E-19	0	0
9.82	0	4.9583E-19	0	0
10.2	0	5.55647E-19	0	0
10.6	0	6.23615E-19	0	0
10.9	171.804	6.78076E-19	2.71824E-15	3.08249E-16
11.3	0	7.55499E-19	0	0
11.8	0	8.6029E-19	0	0
12.2	151.079	9.50776E-19	3.35165E-15	3.80077E-16
12.6	0	1.04739E-18	0	0
13.1	139.539	1.1771E-18	3.83252E-15	4.34608E-16
13.6	0	1.31709E-18	0	0
14.1	513.219	1.46776E-18	1.75766E-14	1.99319E-15
14.6	150.201	1.62951E-18	5.71093E-15	6.47619E-16
15.1	872.427	1.80272E-18	3.66974E-14	4.16149E-15

15.7	46.7028	2.02627E-18	2.20809E-15	2.50398E-16
16.3	219.932	2.26757E-18	1.16366E-14	1.31959E-15
16.8	280.841	2.48271E-18	1.62691E-14	1.84492E-15
17.5	647.81	2.80616E-18	4.24167E-14	4.81006E-15
18.1	852.133	3.10481E-18	6.17332E-14	7.00054E-15
18.8	762.931	3.47914E-18	6.19347E-14	7.0234E-15
19.5	955.049	3.88242E-18	8.65177E-14	9.81111E-15
20.2	485.062	4.31571E-18	4.88457E-14	5.53911E-15
20.9	1938.77	4.78011E-18	2.16242E-13	2.45219E-14
21.7	2750.77	5.3503E-18	3.43407E-13	3.89423E-14
22.5	2490.06	5.96412E-18	3.46524E-13	3.92958E-14
23.3	2808.99	6.62318E-18	4.34104E-13	4.92273E-14
24.1	3302.57	7.32908E-18	5.64779E-13	6.40459E-14
25	3634.54	8.18123E-18	6.93817E-13	7.86788E-14
25.9	4594.65	9.09699E-18	9.75275E-13	1.10596E-13
26.9	6934.37	1.01919E-17	1.64907E-12	1.87005E-13
27.9	8073.75	1.13713E-17	2.14222E-12	2.42927E-13
28.9	9517.19	1.26384E-17	2.80658E-12	3.18266E-13
30	10074.6	1.41372E-17	3.32328E-12	3.7686E-13
31.1	10062	1.575E-17	3.69778E-12	4.19328E-13
32.2	12649.5	1.7481E-17	5.1596E-12	5.85099E-13
33.4	15576.7	1.95091E-17	7.09072E-12	8.04088E-13
34.6	15385	2.16884E-17	7.78576E-12	8.82906E-13
35.9	17367.2	2.4226E-17	9.81722E-12	1.11327E-12
37.2	17531.5	2.69543E-17	1.10261E-11	1.25036E-12
38.5	19971.1	2.988E-17	1.39239E-11	1.57897E-12
40	17890.6	3.35103E-17	1.39888E-11	1.58633E-12

41.4	21251.9	3.71535E-17	1.84236E-11	2.08923E-12
42.9	23677.7	4.134E-17	2.28395E-11	2.59E-12
44.5	23481.7	4.61401E-17	2.52805E-11	2.8668E-12
46.1	22401.6	5.12981E-17	2.68137E-11	3.04068E-12
47.8	21274.8	5.7185E-17	2.83873E-11	3.21912E-12
49.6	22631.1	6.38916E-17	3.37385E-11	3.82595E-12
51.4	21373.2	7.1103E-17	3.54596E-11	4.02112E-12
53.3	22119.2	7.9283E-17	4.09191E-11	4.64023E-12
55.2	22982.2	8.80675E-17	4.72263E-11	5.35547E-12
57.3	23010	9.8506E-17	5.28878E-11	5.99748E-12
59.4	23167.3	1.09738E-16	5.93212E-11	6.72703E-12
61.5	24467.2	1.21793E-16	6.9532E-11	7.88493E-12
63.8	22657.7	1.35975E-16	7.18875E-11	8.15204E-12
66.1	22656.8	1.51218E-16	7.99426E-11	9.06549E-12
68.5	19976.6	1.68295E-16	7.84456E-11	8.89573E-12
71	20052.7	1.87402E-16	8.76846E-11	9.94343E-12
73.7	21544.8	2.09605E-16	1.05371E-10	1.19491E-11
76.4	18922.3	2.33496E-16	1.03093E-10	1.16908E-11
79.1	20014.8	2.59136E-16	1.2102E-10	1.37236E-11
82	17466.4	2.88696E-16	1.17658E-10	1.33424E-11
85.1	17505.9	3.22691E-16	1.3181E-10	1.49473E-11
88.2	17263.1	3.59256E-16	1.4471E-10	1.64102E-11
91.4	15616.2	3.99795E-16	1.45676E-10	1.65197E-11
94.7	16409.4	4.44681E-16	1.70262E-10	1.93077E-11
98.2	13611.5	4.9583E-16	1.57477E-10	1.78578E-11
101.8	13111.5	5.52385E-16	1.68994E-10	1.91639E-11
105.5	12992.4	6.14831E-16	1.8639E-10	2.11366E-11

109.4	10934.3	6.85568E-16	1.74911E-10	1.9835E-11
113.4	10571	7.63551E-16	1.88335E-10	2.13572E-11
117.6	9717.39	8.5157E-16	1.93084E-10	2.18958E-11
121.9	9674.28	9.4844E-16	2.14094E-10	2.42783E-11
126.3	7838.21	1.05489E-15	1.92931E-10	2.18784E-11
131	7810.3	1.1771E-15	2.14515E-10	2.4326E-11
135.8	7874.1	1.31129E-15	2.40922E-10	2.73205E-11
140.7	6451.33	1.45841E-15	2.19537E-10	2.48955E-11
145.9	5965.3	1.62616E-15	2.26346E-10	2.56677E-11
151.2	5062.74	1.8099E-15	2.13804E-10	2.42454E-11
156.8	4759.96	2.01854E-15	2.2419E-10	2.54232E-11
162.5	4298.15	2.24677E-15	2.25329E-10	2.55523E-11
168.5	3643.09	2.50495E-15	2.12934E-10	2.41467E-11
174.7	3762.86	2.79176E-15	2.45116E-10	2.77962E-11
181.1	2350.03	3.10995E-15	1.70531E-10	1.93383E-11
187.7	3063.75	3.46251E-15	2.47526E-10	2.80695E-11
194.6	2569.2	3.85858E-15	2.31314E-10	2.6231E-11
201.7	2141.45	4.29651E-15	2.14685E-10	2.43452E-11
209.1	1748.56	4.78697E-15	1.95307E-10	2.21478E-11
216.7	1236.81	5.32814E-15	1.53764E-10	1.74369E-11
224.7	1340.26	5.94029E-15	1.85769E-10	2.10662E-11
232.9	1544.38	6.61465E-15	2.38363E-10	2.70303E-11
241.4	1007.28	7.36564E-15	1.73116E-10	1.96314E-11
250.3	1103.03	8.21072E-15	2.11322E-10	2.39639E-11
259.5	688.405	9.14978E-15	1.46971E-10	1.66665E-11
269	803.026	1.01919E-14	1.90969E-10	2.16558E-11
278.8	497.683	1.13469E-14	1.31767E-10	1.49424E-11

SUM	848899.4638		7.89509E-09	8.95303E-10

Table 7: Experimental Result for the Total Amount of particles in Negative Corona Charger.

$17000(v)$			
dp	$C,\#/cm\text{^}3$	$dp-v,cm\text{^}3$	$Mass$
7.37	0	2.09605E-19	0
7.64	417.876	2.33496E-19	2.58176E-16
7.91	791.738	2.59136E-19	5.42874E-16
8.2	1246.23	2.88696E-19	9.51981E-16
8.51	2032.04	3.22691E-19	1.73504E-15
8.82	3155.73	3.59256E-19	2.99981E-15
9.14	3472.12	3.99795E-19	3.67301E-15
9.47	6377.69	4.44681E-19	7.50416E-15
9.82	7476.21	4.9583E-19	9.80854E-15
10.2	8762.67	5.55647E-19	1.28832E-14
10.6	10184.3	6.23615E-19	1.6805E-14
10.9	9049.25	6.78076E-19	1.62361E-14
11.3	18686.6	7.55499E-19	3.73555E-14
11.8	33087.2	8.6029E-19	7.53173E-14
12.2	46150.8	9.50776E-19	1.16104E-13
12.6	55094.3	1.04739E-18	1.52689E-13
13.1	77018.6	1.1771E-18	2.39882E-13
13.6	113853	1.31709E-18	3.9678E-13
14.1	129574	1.46776E-18	5.03227E-13
14.6	160337	1.62951E-18	6.91323E-13
15.1	168282	1.80272E-18	8.02707E-13
15.7	291569	2.02627E-18	1.56325E-12
16.3	336208	2.26757E-18	2.01725E-12
16.8	357874	2.48271E-18	2.35097E-12
17.5	432000	2.80616E-18	3.20765E-12
18.1	521534	3.10481E-18	4.28457E-12
18.8	687044	3.47914E-18	6.3248E-12
19.5	696849	3.88242E-18	7.15865E-12
20.2	837569	4.31571E-18	9.56452E-12
20.9	873606	4.78011E-18	1.10495E-11

21.7	1.09E+06	5.3503E-18	1.54786E-11
22.5	1.27E+06	5.96412E-18	2.01174E-11
23.3	1.26E+06	6.62318E-18	2.21387E-11
24.1	1.27E+06	7.32908E-18	2.46044E-11
25	1.44E+06	8.18123E-18	3.11718E-11
25.9	1.58E+06	9.09699E-18	3.81099E-11
26.9	1.66E+06	1.01919E-17	4.48892E-11
27.9	1.83E+06	1.13713E-17	5.51195E-11
28.9	1.63E+06	1.26384E-17	5.45232E-11
30	1.60E+06	1.41372E-17	5.97034E-11
31.1	1.63E+06	1.575E-17	6.79956E-11
32.2	1.50E+06	1.7481E-17	6.92595E-11
33.4	1.42E+06	1.95091E-17	7.30455E-11
34.6	1.35E+06	2.16884E-17	7.74357E-11
35.9	1.26E+06	2.4226E-17	8.08243E-11
37.2	1.05E+06	2.69543E-17	7.49812E-11
38.5	956927	2.988E-17	7.56571E-11
40	953068	3.35103E-17	8.45069E-11
41.4	829157	3.71535E-17	8.15129E-11
42.9	688455	4.134E-17	7.53071E-11
44.5	665728	4.61401E-17	8.12766E-11
46.1	582807	5.12981E-17	7.91072E-11
47.8	490365	5.7185E-17	7.41979E-11
49.6	432000	6.38916E-17	7.30327E-11
51.4	358365	7.1103E-17	6.74223E-11
53.3	280019	7.9283E-17	5.87432E-11
55.2	227628	8.80675E-17	5.30434E-11
57.3	195868	9.8506E-17	5.10524E-11
59.4	164118	1.09738E-16	4.76545E-11
61.5	127572	1.21793E-16	4.11121E-11
63.8	99731.9	1.35975E-16	3.58827E-11
66.1	74100.6	1.51218E-16	2.96493E-11
68.5	61157.1	1.68295E-16	2.72337E-11
71	43354.4	1.87402E-16	2.14979E-11
73.7	30879	2.09605E-16	1.71259E-11

76.4	20629.5	2.33496E-16	1.27455E-11
79.1	13849.8	2.59136E-16	9.49645E-12
82	9697.1	2.88696E-16	7.4075E-12
85.1	5384.59	3.22691E-16	4.59759E-12
88.2	4369.81	3.59256E-16	4.15391E-12
91.4	3720.44	3.99795E-16	3.93569E-12
94.7	2425.44	4.44681E-16	2.85384E-12
98.2	1228.19	4.9583E-16	1.61134E-12
101.8	917.412	5.52385E-16	1.3409E-12
105.5	484.484	6.14831E-16	7.8818E-13
109.4	261.942	6.85568E-16	4.75166E-13
113.4	0	7.63551E-16	0
117.6	52.128	8.5157E-16	1.17458E-13
121.9	0	9.4844E-16	0
126.3	0	1.05489E-15	0
131	104.196	1.1771E-15	3.24529E-13
135.8	52.0874	1.31129E-15	1.80726E-13
140.7	52.3178	1.45841E-15	2.01893E-13
145.9	0	1.62616E-15	0
151.2	52.5392	1.8099E-15	2.5161E-13
156.8	0	2.01854E-15	0
162.5	0	2.24677E-15	0
168.5	0	2.50495E-15	0
174.7	0	2.79176E-15	0
181.1	0	3.10995E-15	0
187.7	0	3.46251E-15	0
194.6	0	3.85858E-15	0
201.7	0	4.29651E-15	0
209.1	0	4.78697E-15	0
216.7	884.539	5.32814E-15	1.24705E-11
224.7	3441.45	5.94029E-15	5.40928E-11
232.9	2174.53	6.61465E-15	3.80594E-11
241.4	937.22	7.36564E-15	1.82659E-11
250.3	433.111	8.21072E-15	9.40958E-12
259.5	511.914	9.14978E-15	1.23936E-11

269	121.029	1.01919E-14	3.26388E-12
278.8	122.318	1.13469E-14	3.67246E-12
289	186.477	1.26384E-14	6.23602E-12
			2.14337E-09